STATE OF THE CLIMATE IN 2022

THE TROPICS

H. J. Diamond and C. J. Schreck, Eds.

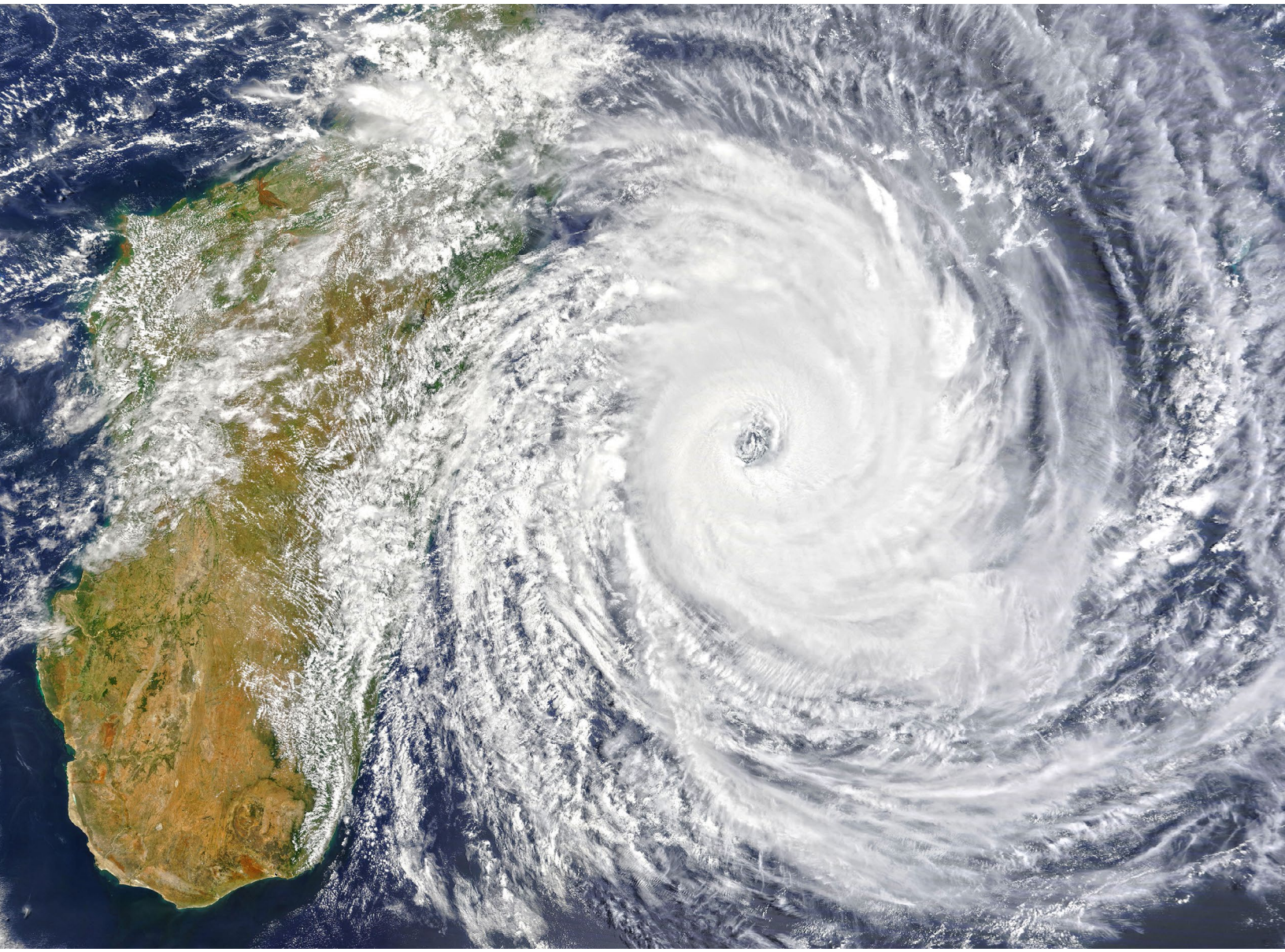

Special Online Supplement to the *Bulletin of the American Meteorological Society* Vol. 104, No. 8, August, 2023

https://doi.org/10.1175/BAMS-D-23-0078.1

Corresponding author: Howard J. Diamond / howard.diamond@noaa.gov

©2023 American Meteorological Society
For information regarding reuse of this content and general copyright information, consult the AMS Copyright Policy.

STATE OF THE CLIMATE IN 2022
The Tropics

Editors

Ellen Bartow-Gillies
Jessica Blunden
Tim Boyer

Chapter Editors

Peter Bissolli
Kyle R. Clem
Howard J. Diamond
Matthew L. Druckenmiller
Robert J. H. Dunn
Catherine Ganter
Nadine Gobron
Gregory C. Johnson
Rick Lumpkin
Ademe Mekonnen
John B. Miller
Twila A. Moon
Marilyn N. Raphael
Ahira Sánchez-Lugo
Carl J. Schreck III
Richard L. Thoman
Kate M. Willett
Zhiwei Zhu

Technical Editor

Lukas Noguchi

BAMS Special Editor for Climate

Michael A. Alexander

American Meteorological Society

Cover Credit:
Hurricane Ian as seen from NOAA's GOES-East satellite on 27 September 2022 at 0826 UTC in the Gulf of Mexico.

(Image credit: NOAA/NESDIS)

How to cite this document:
The Tropics is one chapter from the *State of the Climate in 2022* annual report and is available from https://doi.org/10.1175/BAMS-D-23-0078.1. Compiled by NOAA's National Centers for Environmental Information, *State of the Climate in 2022* is based on contributions from scientists from around the world. It provides a detailed update on global climate indicators, notable weather events, and other data collected by environmental monitoring stations and instruments located on land, water, ice, and in space. The full report is available from https://doi.org/10.1175/2023BAMSStateoftheClimate.1.

Citing the complete report:
Blunden, J., T. Boyer, and E. Bartow-Gillies, Eds., 2023: "State of the Climate in 2022". Bull. Amer. Meteor. Soc., 104 (8), Si–S501 https://doi.org/10.1175/2023BAMSStateoftheClimate.1.

Citing this chapter:
Diamond, H.J. and C. J. Schreck, Eds., 2023: The Tropics [in "State of the Climate in 2022"]. Bull. Amer. Meteor. Soc., 104 (8), S207–S270, https://doi.org/10.1175/BAMS-D-23-0078.1.

Citing a section (example):
Allgood, A. and C. J. Schreck, 2023: Tropical intraseasonal activity [in "State of the Climate in 2022"]. Bull. Amer. Meteor. Soc., 104 (8), S218–S220, https://doi.org/10.1175/BAMS-D-23-0078.1.

Editor and Author Affiliations (alphabetical by name)

Allgood, Adam, NOAA/NWS National Centers for Environmental Prediction Climate Prediction Center, College Park, Maryland

Becker, Emily J., University of Miami Rosenstiel School of Marine and Atmospheric Science, Miami, Florida

Blake, Eric S., NOAA/NWS National Hurricane Center, Miami, Florida

Bringas, Francis G., NOAA/OAR Atlantic Oceanographic and Meteorological Laboratory, Miami, Florida

Camargo, Suzana J., Lamont-Doherty Earth Observatory, Columbia University, Palisades, New York

Chen, Lin, Institute for Climate and Application Research (ICAR)/KLME/ILCEC/CIC-FEMD, Nanjing University of Information Science and Technology, Nanjing, China

Coelho, Caio A.S., Centro de Previsão do Tempo e Estudos Climáticos/National Institute for Space Research, Center for Weather Forecasts and Climate Studies, Cachoeira Paulista, Brazil

Diamond, Howard J., NOAA/OAR Air Resources Laboratory, College Park, Maryland

Fauchereau, Nicolas, National Institute of Water and Atmospheric Research, Ltd., Auckland, New Zealand

Fogarty, Chris, Canadian Hurricane Centre, Dartmouth, Canada

Goldenberg, Stanley B., NOAA/OAR Atlantic Oceanographic and Meteorological Laboratory, Miami, Florida

Goni, Gustavo, NOAA/OAR Atlantic Oceanographic and Meteorological Laboratory, Miami, Florida

Harnos, Daniel S., NOAA/NWS National Centers for Environmental Prediction Climate Prediction Center, College Park, Maryland

He, Qiong, Earth System Modeling Center, Nanjing University of Information Science and Technology, Nanjing, China

Hu, Zeng-Zhen, NOAA/NWS Climate Prediction Center, College Park, Maryland

Klotzbach, Philip J., Department of Atmospheric Science, Colorado State University, Fort Collins, Colorado

Knaff, John A., NOAA/NESDIS Center for Satellite Applications and Research, Fort Collins, Colorado

Kumar, Arun, NOAA/NWS National Centers for Environmental Prediction Climate Prediction Center, College Park, Maryland

L'Heureux, Michelle, NOAA/NWS National Centers for Environmental Prediction Climate Prediction Center, College Park, Maryland

Landsea, Chris W., NOAA/NWS National Hurricane Center, Miami, Florida

Lin, I-I., National Taiwan University, Taipei, Taiwan

Lorrey, Andrew M., National Institute of Water and Atmospheric Research, Ltd., Auckland, New Zealand

Luo, Jing-Jia, Institute for Climate and Application Research, Nanjing University of Information Science and Technology, Nanjing, China

Magee, Andrew D., Centre for Water, Climate and Land, School of Environmental and Life Sciences, University of Newcastle, Callaghan, Australia

Pasch, Richard J., NOAA/NWS National Hurricane Center, Miami, Florida

Pezza, Alexandre B., Greater Wellington Regional Council, Wellington, New Zealand

Rosencrans, Matthew, NOAA/NWS National Centers for Environmental Prediction Climate Prediction Center, College Park, Maryland

Rozkošný, Jozef, Slovak Hydrometeorological Institute, Bratislava, Slovakia

Schreck, Carl J., North Carolina State University, North Carolina Institute for Climate Studies, Cooperative Institute Satellite Earth System Studies, Asheville, North Carolina

Trewin, Blair C., Australian Bureau of Meteorology, Melbourne, Australia

Truchelut, Ryan E., WeatherTiger, Tallahassee, Florida

Wang, Bin, School of Ocean and Earth Science and Technology, Department of Meteorology, University of Hawaii; International Pacific Research Center, Honolulu, Hawaii

Wang, Hui, NOAA/NWS National Centers for Environmental Prediction Climate Prediction Center, College Park, Maryland

Wood, Kimberly M., Department of Geosciences, Mississippi State University, Mississippi State, Mississippi

Editorial and Production Team

Allen, Jessicca, Graphics Support, Cooperative Institute for Satellite Earth System Studies, North Carolina State University, Asheville, North Carolina

Camper, Amy V., Graphics Support, Innovative Consulting and Management Services, LLC, NOAA/NESDIS National Centers for Environmental Information, Asheville, North Carolina

Haley, Bridgette O., Graphics Support, NOAA/NESDIS National Centers for Environmental Information, Asheville, North Carolina

Hammer, Gregory, Content Team Lead, Communications and Outreach, NOAA/NESDIS National Centers for Environmental Information, Asheville, North Carolina

Love-Brotak, S. Elizabeth, Lead Graphics Production, NOAA/NESDIS National Centers for Environmental Information, Asheville, North Carolina

Ohlmann, Laura, Technical Editor, Innovative Consulting and Management Services, LLC, NOAA/NESDIS National Centers for Environmental Information, Asheville, North Carolina

Noguchi, Lukas, Technical Editor, Innovative Consulting and Management Services, LLC, NOAA/NESDIS National Centers for Environmental Information, Asheville, North Carolina

Riddle, Deborah B., Graphics Support, NOAA/NESDIS National Centers for Environmental Information, Asheville, North Carolina

Veasey, Sara W., Visual Communications Team Lead, Communications and Outreach, NOAA/NESDIS National Centers for Environmental Information, Asheville, North Carolina

displaced approximately 5000 people, who took shelter at numerous evacuation centers across Fiji's Western, Central, and Northern Divisions. Damage in Fiji from Cody was estimated at $25 million (U.S. dollars).

The season's second severe tropical cyclone, Dovi, originated as a tropical low in the eastern Coral Sea. The system initially tracked eastward towards Vanuatu, slowed, and began to intensify near Southern Vanuatu. On 9 February, the tropical low was named Tropical Cyclone Dovi and tracked to the south as a Category 1 system. As Dovi continued to intensify, it passed off the east coast of New Caledonia as a Category 3 system on 10 February. Dovi reached its peak intensity as an Australian Category 4 storm with sustained winds of 95 kt (49 m s^{-1}) and a minimum central pressure of 940 hPa on 11 February. Dovi then passed west of Norfolk Island and continued to track south, transitioning to a subtropical system as it approached New Zealand. The severe tropical cyclone caused significant flooding and power outages in Vanuatu and New Caledonia. The North Island of New Zealand was severely impacted by Dovi after it became an ex-tropical cyclone, particularly in the Bay of Plenty and Hawke's Bay regions where a significant number of homes were damaged. The strong winds from this decaying system caused power and communication lines to be disrupted, leaving many residents without electricity or phone services. High winds also closed the Auckland Harbour Bridge, which is a main thoroughfare. In addition, the water supply was compromised in the town of Featherston during this storm, and uprooted trees and broken tree limbs resulted in damage to water and road infrastructure. Approximately $35 million (U.S. dollars) in damage was attributed to Dovi in New Zealand alone.

One out-of-season TC occurred in May: Tropical Cyclone Gina. Forming approximately 400 km northeast of Port Vila, Vanuatu, in an area of favorable oceanic (SSTs around 30°C) and environmental (low-to-moderate vertical wind shear) conditions, the tropical depression continued to intensify as it tracked westward towards Vanuatu. On 18 May, Gina reached maximum intensity of 35 kt (18 m s^{-1}) and a minimum central pressure of 998 hPa and maintained Category 1 intensity for approximately 48 hours, continuing to track towards the southeast. Prolonged and intense rainfall from Gina caused flooding in parts of Vanuatu and resulted in the temporary closure of Port Vila's Bauerfield Airport.

h. Tropical cyclone heat potential

—F. Bringas, G. J. Goni, I-I Lin, and J. A. Knaff

Tropical cyclone heat potential (TCHP; e.g., Goni et al. 2009, 2017) is an indicator of the available heat stored in the upper ocean that can potentially induce tropical cyclone (TC) intensification and regulate ocean–atmosphere enthalpy fluxes and TC-induced sea-surface temperature (SST) cooling (e.g., Lin et al. 2013). TCHP is calculated as the integrated heat content between the sea surface and the 26°C isotherm (D26), which is generally taken to be the minimum temperature required for TC genesis and intensification (Leipper and Volgenau 1972; Dare and McBride 2011).

Provided that atmospheric conditions are favorable, TC intensification, including rapid intensification, has been associated with areas in the ocean that have TCHP values above 50 kJ cm^{-2} (e.g., Shay et al. 2000; Mainelli et al. 2008; Lin et al. 2014, 2021; Knaff et al. 2018, 2020). High SSTs prior to TC formation usually lead to less SST cooling during the lifetime of the TC, and hence higher enthalpy fluxes from the ocean into the storm, which favors intensification (e.g., Lin et al. 2013). Similarly, upper-ocean salinity is another condition of relevance for TC intensification because fresh water-induced barrier layers may also modulate the upper-ocean mixing and cooling during a TC and thus the air–sea fluxes (e.g., Balaguru 2012; Domingues et al. 2015). Upper-ocean thermal conditions observed during 2022 are presented here in terms of two parameters: 1) TCHP anomaly values with respect to their long-term mean (1993–2020) and 2) TCHP anomaly values compared to conditions observed in 2021. TCHP anomalies during 2022 (Fig. 4.41) are computed for June–November in the Northern Hemisphere and November 2021–April 2022 in the Southern Hemisphere. In Fig. 4.41, the seven regions where TCs are known to form, travel, and intensify are highlighted. In all of these regions, TCHP values exhibit large

temporal and spatial variability due to mesoscale features, trends, and short- to long-term modes of variability, such as the North Atlantic Oscillation, El Niño–Southern Oscillation (ENSO), and the Pacific Decadal Oscillation. The differences in TCHP anomalies between 2021 and 2022 are also computed for the primary months of TC activity in each hemisphere (Fig. 4.42).

During 2022, TCHP anomaly conditions were above average for most TC regions and basins, with the exception of the eastern North Pacific, the southern portion of the South Indian, and near the center of the North Atlantic Gyre (Fig. 4.41). In particular, some areas in the North Indian Ocean, western North Pacific Ocean, east and west of Australia, and portions of the North Atlantic Ocean exhibited TCHP anomaly values above 30 kJ cm^{-2}, which are indicative of favorable oceanic conditions for the development and intensification of TCs.

Compared to 2021, TCHP anomalies during 2022 were larger in some regions of the western North Pacific and North Atlantic, most of the Gulf of Mexico, and much of the Southern Hemisphere. They were notably smaller in the central and eastern Pacific. These lower TCHP anomalies during 2022 were associated with the ongoing and stronger negative phase of ENSO (La Niña), prevalent in this region since mid-2021 (Fig. 4.42). In the Southern Hemisphere, TCHP anomalies during 2022 were average or above average, with values above 30 kJ cm^{-2} in small areas in the South Indian Ocean and more extended areas in the southwestern Pacific (Fig. 4.41). TCHP anomalies in 2022 were on average similar to those observed in 2021 in most of the Southern Hemisphere, with most areas showing differences between ±10 kJ cm^{-2}, except for the southwestern Pacific (Fig. 4.42).

In the South Indian Ocean basin, the most intense storm of the season was Batsirai, which after being named on 28 January, underwent several periods of intensification and weakening until experiencing rapid intensification from Category 2 to Category 4 on 2 February, when it reached its peak intensity of 125 kt (64 m s^{-1}) and a minimum central barometric pressure of 932 hPa, while traveling over a region with SST >27°C and TCHP >50 kJ cm^{-2}. Similar to Batsirai, Cyclone Gombe underwent rapid intensification on 9 March over a period of 18 hours while traveling over the Mozambique Channel with SST >30°C and TCHP >80 kJ cm^{-2}, reaching peak intensity of 110 kt (57 m s^{-1}) and a minimum central barometric pressure of 959 hPa.

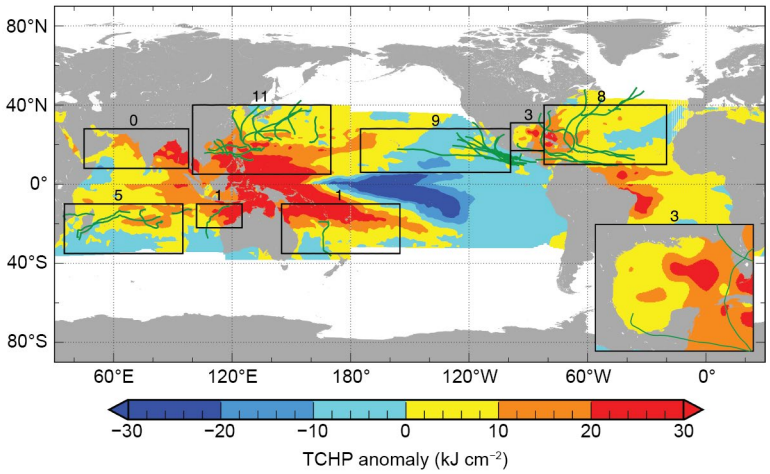

Fig. 4.41. Global anomalies of tropical cyclone heat potential (TCHP; kJ cm^{-2}) during 2022. The boxes indicate the seven regions where TCs occur: from left to right, southwest Indian, North Indian, west North Pacific, southeast Indian, South Pacific, east Pacific, and North Atlantic (shown as Gulf of Mexico and tropical Atlantic separately). The green lines indicate the trajectories of all tropical cyclones reaching at least Category 1 intensity (one-minute average wind ≥64 kt, 34 m s^{-1}) and above during Nov 2021–Apr 2022 in the Southern Hemisphere and Jun–Nov 2022 in the Northern Hemisphere. The numbers above each box correspond to the number of Category 1 and above cyclones that traveled within that box. The Gulf of Mexico conditions are shown in the inset in the lower right corner.

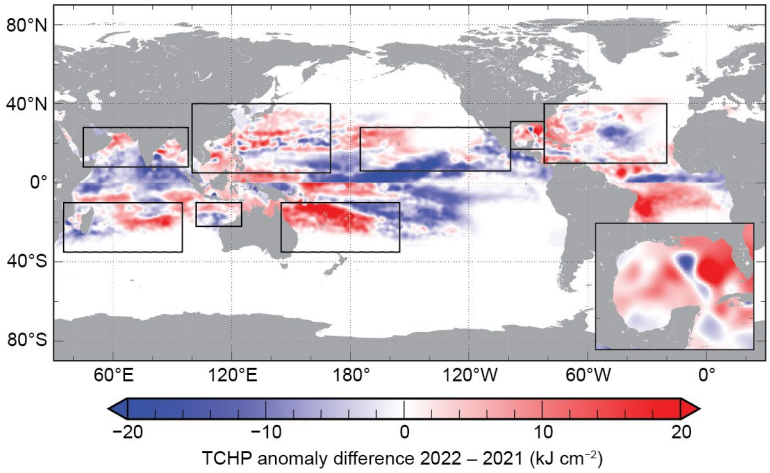

Fig. 4.42. Tropical cyclone heat potential (TCHP) anomaly difference between the 2022 and 2021 tropical cyclone seasons (kJ cm^{-2}; Jun–Nov in the Northern Hemisphere and Nov–Apr in the Southern Hemisphere). The Gulf of Mexico conditions are shown in the inset in the lower right corner.

Large positive areas of high TCHP anomaly values were observed in the regions east and west of Australia where TCs typically translate. However, in 2021/22, below-average TC activity was observed in these two regions with a total of 10 TCs, of which only 2 reached Category 1 intensity or above.

Similar to the eastern and western Australia regions, the North Indian Ocean experienced above-average TCHP anomalies in excess of 30 kJ cm^{-2} during 2022 in the Bay of Bengal and northern Arabian Sea. No Category 1 or above storms were recorded during June–November (Fig. 4.41), which made for a below-average season in terms of TC intensity. One caveat associated with this result is that almost all TCs forming in this region do so during the pre- and post-monsoon seasons (May–June and October–December).

In the western North Pacific basin, the upper-ocean thermal conditions are largely modulated by the state of ENSO (e.g., Lin et al. 2014, 2020; Zheng et al. 2015). During all of 2022, La Niña was observed in this region with TCHP anomalies that were positive in the western North Pacific, with values well above 30 kJ cm^{-2} closer to the equator and a regional average of approximately 20 kJ cm^{-2} when compared to the long-term mean (Fig. 4.41), as is typical in a La Niña year (Lin et al. 2014; 2020). TCHP anomalies in the western North Pacific were fairly similar in 2021 and 2022, likely due to the predominance of La Nina conditions in both years (Fig. 4.42). Due to the influence of La Niña, TC activity during 2022 was below average for the western North Pacific. Nevertheless, there were two notable super typhoons: Hinnamnor and Nanmadol. Hinnamnor originated and intensified to Category 5 (140 kt; 72 m s^{-1}) over a region of high TCHP (>60 kJ cm^{-2}), though at relatively high latitudes (~22°N–26°N). The storm reached its lifetime maximum intensity (LMI) of 140 kt (72 m s^{-1}) on 30 August. After a short period of intensity fluctuation to ~125 kt (64 m s^{-1}), Hinnamnor intensified back to 140 kt on 1 September. The most noteworthy feature in Hinnamnor was its sharp 90° turn in its track that was accompanied by dramatic reduction of its forward motion to near-stationary (i.e., ~1 m s^{-1} to 2 m s^{-1}) on 1–2 September. As a result of this slowing, a large cold pool was induced and contributed to Hinnamnor's weakening to ~75 kt (39 m s^{-1}). Super Typhoon Nanmadol also originated and intensified over areas with TCHP >50 kJ cm^{-2}, and similarly at a relatively high latitude of ~21°N–26°N. It reached its LMI of 135 kt (69 m s^{-1}) on 16 September. After LMI, Nanmadol maintained a northwest track while steadily weakening before it made landfall in Japan and affected both Japan and South Korea.

In the North Atlantic basin, upper-ocean thermal conditions during the 2022 hurricane season were characterized by TCHP anomalies larger than the long-term average except in areas of the eastern portion of this region, west of Africa, with values on the western part of the basin of around 20 kJ cm^{-2} on average for most of the region and up to 30 kJ cm^{-2} in smaller areas around Cuba (Fig. 4.41). TCHP anomalies were also positive during 2022 in areas associated with the location of the Loop Current's northern extension in the Gulf of Mexico, where these anomalies were greater than 25 kJ cm^{-2} during 2022 compared to the long-term mean. Differences of ±20 kJ cm^{-2} between 2022 and 2021 were observed, likely as a result of the variability of ocean currents in the region.

Hurricane Fiona formed during 12–14 September, despite environmental conditions considered to be only marginally favorable. The system became a named storm on 15 September while moving towards the Caribbean Sea region. After becoming a Category 3 hurricane, Fiona traveled over Puerto Rico and the Dominican Republic, where it weakened slightly, but emerged in the tropical North Atlantic and intensified into a Category 4 TC on 21 September. Fiona reached peak intensity of one-minute sustained wind speeds of 115 kt (58 m s^{-1}) and a minimum central barometric pressure of 932 hPa while traveling over a region with SST >30°C and TCHP >80 kJ cm^{-2}, which is well above the 50-kJ cm^{-2} threshold required to support Atlantic hurricane intensification (Mainelli et al. 2008).

Major Hurricane Ian, the most intense Atlantic storm in 2022, reached Category 1 intensity on 26 September, and intensified to a Category 3 system while approaching the southwestern tip of Cuba. Ian continued traveling north into the Gulf of Mexico, where on 28 September it

strengthened into a Category 5 hurricane with peak intensity of one-minute sustained wind speeds of 140 kt (72 m s^{-1}) and minimum central barometric pressure of 936 hPa, while traveling over a region with SST >31°C and TCHP > 115 kJ cm^{-2}. Ian then made landfall as a Category 4 hurricane in Florida.

In summary, favorable upper-ocean thermal conditions were observed in all TCHP basins during the 2022 season, except in the eastern North Pacific, where conditions were slightly below average compared to the long-term mean. Additionally, TCHP anomaly values during 2022 exhibited generally similar values in most regions compared to the previous year in most basins, with higher values reported in the western North Atlantic and the eastern Australia regions. This translated into above-average hurricane activity in the South Indian region, average activity in the North Atlantic and eastern North Pacific, and below-average activity in the northwest Pacific and North Indian Oceans. Several significant storms, including Intense Cyclones Batsirai and Gombe in the southwestern Indian Ocean, Super Typhoons Hinnamnor and Nanmadol in the western North Pacific, and Major Hurricanes Fiona and Ian in the North Atlantic, Caribbean Sea, and Gulf of Mexico, underwent rapid intensification while traveling over areas with favorable ocean conditions including high TCHP values.

Sidebar 4.1: Hurricanes Fiona and Ian: A pair of impactful North Atlantic major hurricanes

—C. FOGARTY, R. TRUCHELUT, AND P. KLOTZBACH

Both major hurricanes that formed during the 2022 Atlantic hurricane season (Fiona and Ian) caused tremendous damage and loss of life. This sidebar details the meteorology and briefly summarizes the impacts that these storms caused. Here we highlight the damage that Fiona caused in the Atlantic Provinces of Canada and that Ian caused in Florida. We also note that Fiona also caused massive flooding damage in Puerto Rico, and Ian caused significant wind and storm surge damage in Cuba. Observed statistics are taken from the National Hurricane Center (NHC)'s Tropical Cyclone Reports on Fiona (Pasch et al. 2023) and Ian (Bucci et al. 2023).

Hurricane Fiona developed from a tropical wave off the coast of Africa, reaching tropical depression status ~8000 km east of Guadeloupe on 14 September. Later that day, the NHC designated the system Tropical Storm Fiona, and on 18 September an eye formed, with Fiona reaching hurricane status as it approached southwestern Puerto Rico, where it caused heavy flooding and severe power outages. The storm reached major hurricane status on 20 September while traversing the eastern Bahamas. Fiona reached its peak intensity as a Category 4 storm (120 kt; 62 m s^{-1}) with a minimum pressure as a tropical system of 931 hPa 42 hours later as it tracked just northwest of Bermuda. The pressure rose to 940 hPa after Fiona passed Bermuda, and then the system underwent a volatile extratropical transition process late on 23 September and early on 24 September while still maintaining winds of Category 3 intensity (100 kt; 51 m s^{-1}). During the early hours of 24 September, Fiona made landfall in eastern Nova Scotia as a Category 2-force severe post-tropical cyclone with a minimum sea-level pressure of 931 hPa—the lowest ever recorded sea-level pressure of any cyclone over land in Canada. The storm rapidly accelerated as it approached Nova Scotia, then slowed significantly near Cape Breton. Fiona weakened as it moved slowly northward through the Gulf of St. Lawrence on 25 September and into the Labrador Sea. Fiona dissipated by 28 September.

Fiona was the most intense and most destructive tropical or post-tropical cyclone in Atlantic Canada's history. The extratropical transition (ET) was truly remarkable since an approaching upper-level potential vorticity anomaly interacted with the storm while it was still a major hurricane. The cloud and wind field expanded exceptionally quickly, with most of the ET process occurring over a 12-hour period from 1200 UTC on 23 September to 0000 UTC on 24 September. The damage swath of the storm was immense and occurred not just over the eastern (right-of-track) sector, but also over a large region west of the track where, in fact, the highest winds were observed (Fig. SB4.1). These winds were actually from the baroclinic energetics portion of the storm and were more persistent and produced greater storm surge than on the east side. The slow forward motion of Fiona worsened the impacts overall. Trapped-fetch wave growth (Bowyer and MacAfee 2005) east of the track over parts of northern Cape Breton and southwestern Newfoundland caused extensive damage and was responsible for the complete destruction of numerous homes